# Pitch-angle Scattering vs. Magnetic Confinement in Flare Loops


Jabus van den Berg[1,2], Frederic Effenberger[3,4] and Du Toit Strauss[1]

[1] Centre for Space Research, North-West University, Potchefstroom, South Africa; 24182869@nwu.ac.za
[2] South African National Space Agency, Hermanus, South Africa
[3] Institut für Theoretische Physik, Ruhr-Universität Bochum, Bochum, Germany
[4] Bay Area Environmental Research Institute, NASA Research Park, Moffett Field, CA, USA



**Abstract**

Accelerated particles in flaring loops are confined by both pitch-angle scattering and the converging of magnetic fields to the loop endpoints, i.e. magnetic mirroring. This confinement, together with the initial pitch-angle distribution of the injected particles, governs the average escape time of particles from the loop. The escape time can give an estimate of the particle spectrum as it indicates how much time is available for acceleration and energy losses to occur. Pitch-angle scattering is caused by both Coulomb collisions and magnetic turbulence, but the two processes have different pitch-angle and energy dependencies, and could therefore yield different escape times. The hard X-rays produced by escaping particles are sensitive to the temporal profile and pitch-angle distribution of escaping particles and not the average escape time. We investigate the effect of a spatially varying magnetic field and anisotropic scattering on the escape time. We find that these considerations only yield a factor two difference in the escape time compared to isotropic scattering in a uniform magnetic field with a loss cone specified at the endpoints. The temporal profile and pitch-angle distribution of escaping particles are also investigated. We find that the time when the bulk of the particles escape can be quite different from the average escape time and that periodic 'waves' of escaping particles are found under weak scattering conditions. The pitch-angle distributions of escaping particles are found to be generally neither isotropic nor beamed, and critically depend on either the scattering regime or the injected distribution.


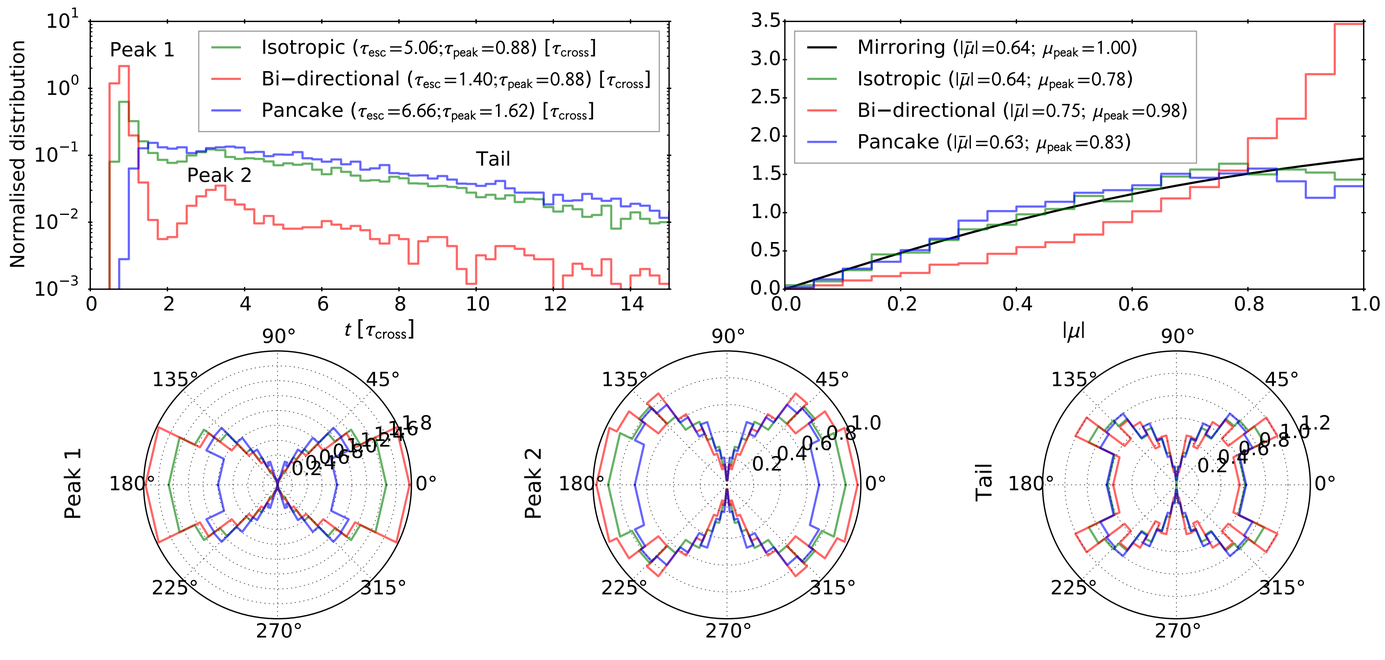


**Fig. 3:** *Temporal profile* **(top left)** *and time integrated pitch-angle distribution (PAD)* **(top right)** *of escaping particles for $n = 2$, $\eta = 2$, and isotropic scattering with $D_0 \approx 0.2$ (intermediate scattering: $\tau_{sc} \sim \tau_{cross}$). The distributions' average and the values where the distributions peak are indicated in the legends. Only $|\mu|$ is considered for the time integrated PAD because the PAD at the two endpoints are symmetric about $\mu = 0$. The PAD at three different times (indicated in the time profile) are shown in the* **bottom row** *as polar plots (0° being in the direction of the magnetic field and 180° being in the opposite direction; the right/left hemisphere corresponds to particles escaping at $s = s_m/s = -s_m$).*

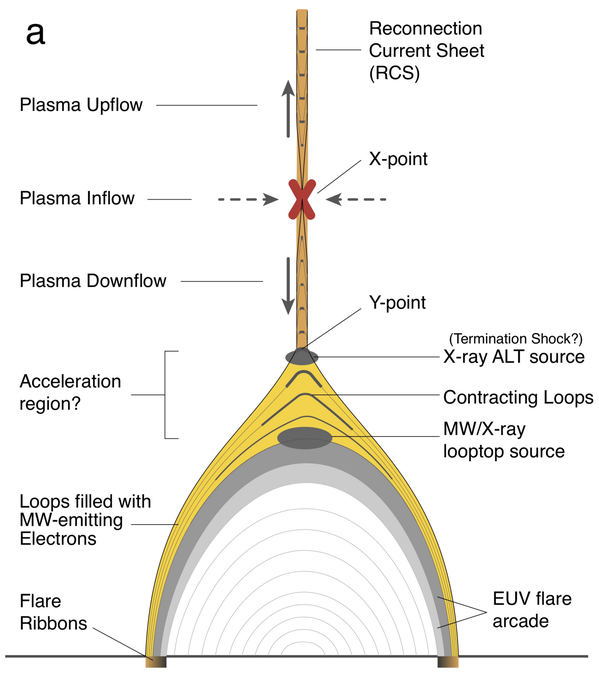


**Fig. 1:** *Cartoon representation of the standard flare model by Yu et al. [2020]. Figure taken from* `http://www.astro.gla.ac.uk/cartoons/`

## 1 Background

Fig. 1 shows a cartoon of the standard flare model. Particles are accelerated somewhere in the reconnection current sheet and probably the loop top, and stream down to the foot points where they are either mirrored back into the loop by the converging magnetic field or escape and produce hard x-rays (HXRs) in the dense chromosphere through Bremsstrahlung to form the flare ribbons. Some of these particles, however, must also escape into the less dense upper corona to form solar energetic particles (SEPs) where the propagation effects are different, i.e. magnetic turbulence plays a more important role compared to Coulomb collisions. We are interested in the relationship between particles producing HXRs and the observed SEPs: i.e. What fraction of particles are released as SEPs? What is the correlation between the HXR spectrum or time profile and that of SEPs?

In order to build a conceptual understanding of the effects of different processes, we focus here on particles trapped in the flare's lower loop and extended the 1D model of *Effenberger & Petrosian [2018]* to specifically investigate the effect of a spatially varying magnetic field and isotropic vs. anisotropic pitch-angle scattering.

## 2 Model

### 2.1 Governing Equations

We solved, with stochastic differential equations *[see e.g. Strauss & Effenberger, 2017]*, the focused transport equation of *Roelof [1969]* for the distribution function $f(s;\mu;t)$,

$$\frac{\partial f}{\partial t} + \frac{\partial}{\partial s}\left[\mu v\, f\right] + \frac{\partial}{\partial \mu}\left[\frac{\left(1-\mu^2\right) v}{2L(s)} f\right] = \frac{\partial}{\partial \mu}\left[D_{\mu\mu}\frac{\partial f}{\partial \mu}\right], \tag{1}$$

where $s$ is the coordinate along the magnetic field line, $v$ is the particle's speed, $\mu$ is the cosine of the particle's pitch-angle, $L(s)^{-1} = -d\ln B(s)/ds$ is the focusing length of the magnetic field, and $D_{\mu\mu}(\mu)$ is the pitch-angle diffusion coefficient. The initial distribution was chosen as

$$f(s=0;\mu;t=0) = \delta(s)\delta(t)\begin{cases} \mu \sim \mathcal{U}[-1;1] & \text{isotropic} \\ \delta(\mu \pm 1) & \text{bi}-\text{directional beam} \\ \delta(\mu) & \text{pancake} \end{cases},$$

where $\sim \mathcal{U}$ indicates a uniform distribution.

### 2.2 Magnetic Field

$$B(s) = B_0\left[1 + (\eta - 1)\left|\frac{s}{s_m}\right|^n\right] \tag{2}$$

$$L(s) = -\frac{\text{sign}(s)}{n}\left[\frac{s_m^n}{(\eta-1)|s|^{n-1}} + |s|\right] \tag{3}$$

where $B_0 = B(0)$ is the field strength at the loop mid point, $s_m = \ell/2$ is the loop end point, with $\ell$ the loop length, $\eta = B(s_m)/B_0$ is the mirror ratio, and $n$ controls how quickly or gradually the magnetic field changes with $s$.

### 2.3 Pitch-angle scattering

- Isotropic scattering, e.g. due to Coulomb collisions,

$$D^{\text{iso}}_{\mu\mu}(\mu) = D_0(1-\mu^2). \tag{4}$$

- Anisotropic scattering, e.g. due to turbulence,

$$D^{\text{aniso}}_{\mu\mu}(\mu) = D_\epsilon(1-\mu^2)\left(\frac{|\mu|}{1+|\mu|} + \epsilon\right), \tag{5}$$

where $\epsilon \approx 0.045$ for a Kolmogorov inertial range with dynamical effects *[Agueda et al., 2008]*.
- $D_0$ and $D_\epsilon$ are normalised to the same parallel mean free path *[Hasselmann & Wibberenz, 1970]*,

$$\lambda_\parallel = \frac{3}{8}v\int_{-1}^{1}\frac{\left(1-\mu^2\right)^2}{D_{\mu\mu}(\mu)}d\mu, \tag{6}$$

to yield the same scattering time.

## 3 Results

- Fig. 2 shows the effect of a spatially varying magnetic field and anisotropic scattering on the average escape time.
- Fig. 3 shows the escaping particles' temporal profile and both the time integrated and temporal evolution of the pitch-angle distribution (PAD).
- Time integrated PADs: 1) Strong scattering and intermediate scattering with $\eta = 1$: $\approx 3\mu^2$ or $\approx 2|\mu|$ for isotropic or anisotropic scattering, respectively; 2) Intermediate to weak scattering with $\eta > 1$: $\approx |\mu|/\eta(1-\mu_c)\sqrt{\mu_c^2+\mu^2}/\eta$, with $\mu_c = \sqrt{1-\eta^{-1}}$; 3) Too weak scattering: $\approx \delta(|\mu|-1)$ or $\approx 3(2\mu_{\text{peak}}|\mu| - \mu^2)/4\mu^3_{\text{peak}}$ for bi-directional beam or pancake injection, respectively, with $\mu_{\text{peak}} \propto n\eta(\tau_{\text{cross}}/\tau_{\text{sc}})$; 4) Too weak scattering with isotropic injection: almost isotropic with depletion towards $\mu = 0$ if $\eta = 1$ and converges to the pancake's PAD as $\eta$ increases.
- Fig. 4 shows the escaping particles' pitch-cosines as a function of their escape time. The 'waves' of escaping particles in the intermediate and weak scattering regimes have periods of $\sim 1.4 - 2.7\,\tau_{\text{cross}}$, depending on $n$ and $\eta$.

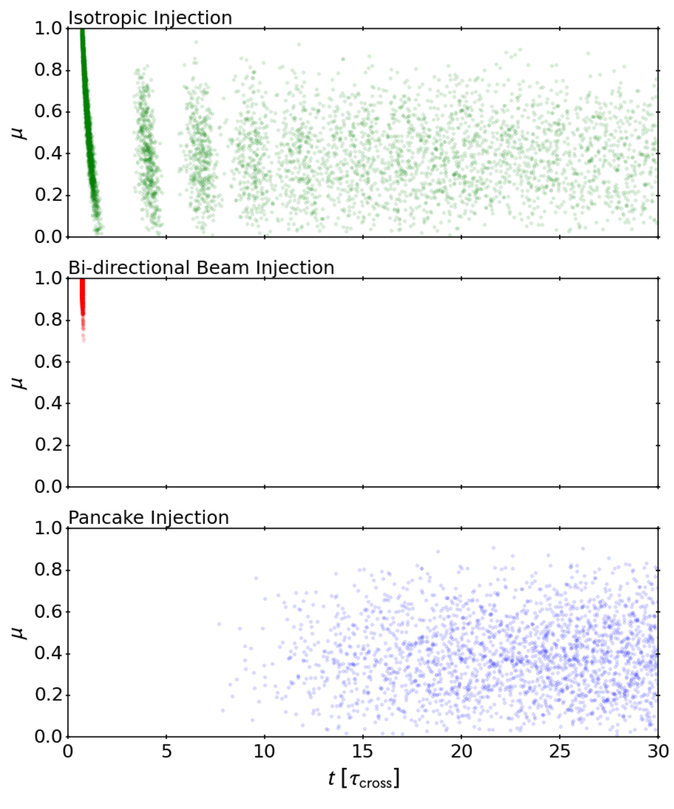


**Fig. 4:** *$|\mu|$ of escaping particles as a function of their escape time for three different injections (isotropic injection* **top***; bi-directional beam injection* **middle***; pancake injection* **bottom***), $n = 2$, $\eta = 2$, and anisotropic scattering with $D_0 \approx 0.007$ (weak scattering).*

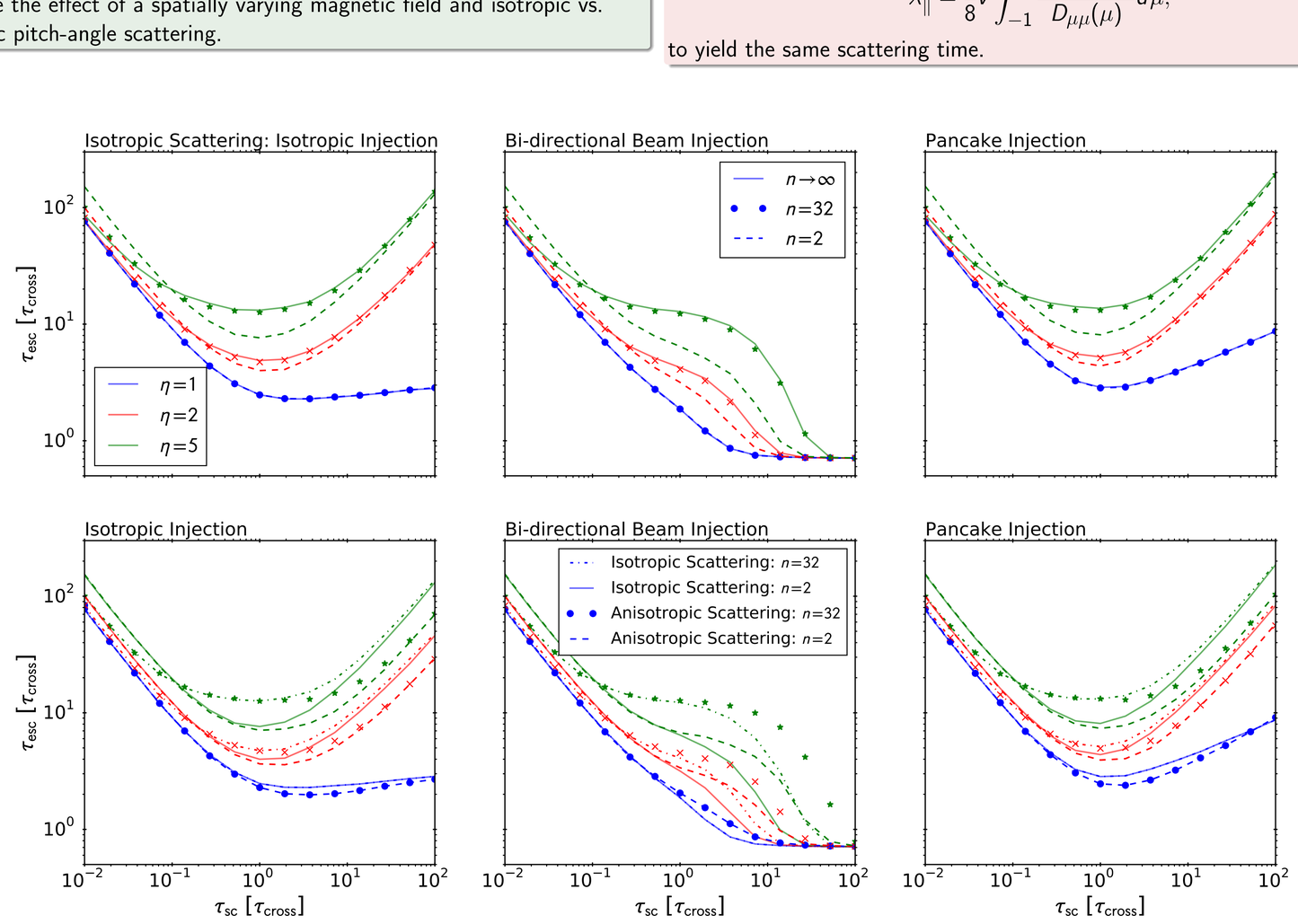


**Fig. 2:** *Average particle escape times as a function of scattering time ($\propto D_0^{-1}$ or $\propto D_\epsilon^{-1}$) for three different injections (isotropic injection* **left***; bi-directional beam injection* **middle***; pancake injection* **right***) and mirror ratios ($\eta = 5$ green; $\eta = 2$ red; $\eta = 1$ blue). Times are normalised to the crossing time ($\propto \ell/v$).* **Top row:** *Isotropic scattering for the model of Effenberger & Petrosian [2018] without a spatially varying magnetic field (solid lines) and a magnetic field with $n = 32$ (symbols) and $n = 2$ (dashed lines).* **Bottom row:** *A magnetic field with $n = 32$ (symbols) and $n = 2$ (dashed lines) for anisotropic scattering. The isotropic scattering results are shown by the solid ($n = 2$) and dashed-dotted ($n = 32$) lines for comparison.*

## Conclusions

- Spatially varying magnetic field: 1) traps particles in strong scattering regime; 2) aids particles to escape in intermediate scattering regime.
- Anisotropic scattering: aids particles to escape in weak scattering regime.
- Average escape time only changes by a factor $\sim 2$ when a spatially varying magnetic field and/or anisotropic scattering is present, compared to isotropic scattering in a homogeneous magnetic field with a loss cone at the endpoints.
- Temporal profile of escaping particles: 1) relatively quick rise time followed by slow decay phase; 2) most probable escape time can be quite different from the average escape time; 3) can have multiple peaks due to periodic escape of particles in weak scattering regime.
- Pitch-angle distribution of escaping particles: 1) evolve from beamed to more isotropic over time; 2) shows depletion around 90° pitch-angles; 3) generally neither isotropic nor beamed.
- Both the time profile and time integrated pitch-angle distribution of escaping particles depend on the injected particles' pitch-angle distribution, the scattering regime, and the magnetic field.

### References


- Agueda, N., et al. 2008, ApJ, 675, 1601
- Effenberger, F. & Petrosian, V. 2018, ApJL, 868, L28
- Hasselmann, K. & Wibberenz, G. 1970. ApJ, 162, 1049
- Roelof, E. C. 1969, Lectures in High-Energy Astrophysics, 111
- Strauss, R. D. & Effenberger, F. 2017. SSRv, 212, 151
- Yu, S., et al. 2020, ApJ, 900(1), 17



*This work is based on the research supported in part by the National Research Foundation (NRF) of South Africa (grant nos. 120847, 120345, and 119424) and NASA (grant no. NNX17AK25G). Opinions expressed and conclusions arrived at are those of the authors and are not necessarily to be attributed to the NRF. Additional support from the South African National Space Agency (SANSA), the German science foundation (DFG), and an Alexander von Humboldt group linkage program is also acknowledged.*